A novel approach to improve GNSS Precise Point Positioning during strong ionospheric scintillation: theory and demonstration

B. C. Vani, B. Forte, J. F. G. Monico, S. Skone, M. H. Shimabukuro, A. O. Moraes, I. P. Portella, H. A. Marques

***Abstract*—At equatorial latitudes, ionospheric scintillation is the major limitation in achieving high-accuracy GNSS positioning. This is because scintillation affects the tracking ability of GNSS receivers causing losses of lock and degradation on code pseudorange and carrier phase measurements, thus degrading accuracy. During strong ionospheric scintillation, such effects are more severe and GNSS users cannot rely on the integrity, reliability and availability required for safety-critical applications. In this paper, we propose a novel approach able to greatly reduce these effects of scintillation on Precise Point Positioning (PPP). Our new approach consists of three steps: a) a new functional model that corrects the effects of range errors in the observables; b) a new stochastic model that uses these corrections to generate more accurate positioning; and c) a new strategy to attenuate the effects of losses of lock and consequent ambiguities re-initializations that are caused by the need to re-initialize the tracking. We demonstrate the effectiveness of our method in an experiment using a 30-day static dataset affected by different levels of scintillation in the Brazilian south-eastern region. Even with limitations imposed by data gaps, our results demonstrate improvements of up to 80% in the positioning accuracy. We show that, in the best cases, our method can completely negate the effects of ionospheric scintillation and can recover the original PPP accuracy that would have existed without any scintillation. The significance of this work lies in the improvement it offers in the integrity, reliability and availability of GNSS services and applications.**

***Index Terms*—Ionospheric Scintillation; Mitigation; Precise Point Positioning (PPP); Scintillation-induced Error.**

B. C. Vani was with Graduate Program in Cartographic Sciences, Sao Paulo State University (UNESP), Faculty of Science and Technology, Pres. Prudente. Rua Roberto Simonsen, 305, 19060-900 - Pres. Prudente/SP - Brazil. He is with the Federal Institute of Education, Science and Technology of Sao Paulo (IFSP), R. Jose Ramos Junior, 2750, 19470-000 - Pres. Epitacio/SP - Brazil (e-mail: brunovani@ifsp.edu.br).

B. Forte is with University of Bath, Cleverton Down, BA2 7AY, Bath - United Kingdom (e-mail: B.Forte@bath.ac.uk).

J. F. G. Monico is with Department of Cartography, Sao Paulo State University (e-mail: galera.monico@unesp.br).

S. Skone is with Department of Geomatics Engineering, University of Calgary, Canada (e-mail: shskone@ucalgary.ca).

M. H. Shimabukuro is with Department of Mathematics and Computer Science, Sao Paulo State University (e-mail: milton.h.shimabukuro@unesp.br).

A. O. Moraes is with Instituto de Aeronáutica e Espaço (IAE) and Instituto Tecnológico da Aeronáutica (ITA), Praça Marechal Eduardo Gomes, 50 - Sao José dos Campos/SP, Brazil (e-mail: aom@ita.br).

I. P. Portella is with Instituto Tecnológico da Aeronáutica (e-mail: igorp-portella@gmail.com).

H. A. Marques is with Military Engineering Institute - Praça Gen. Tibúrcio, 80 - Urca, Rio de Janeiro/RJ - Brazil (e-mail: haroldoh2o@gmail.com).

Manuscript received XXX, XX, 2015; revised XXX, XX, 2015.

I. Introduction

At equatorial latitudes, GNSS signals propagating through ionospheric irregularities drifting across the ray path can experience fading in the signal intensity and temporal fluctuations in the signal phase. These effects are known as ionospheric scintillation. In Brazil, ionospheric scintillation can be considered the major limitation for high precise GNSS positioning approaches such as Precise Point Positioning (PPP) and Real-Time Kinematic (RTK). Several fields of operations, like offshore oil exploration, precision agriculture, mining, autonomous navigation and aviation are drastically affected in periods and regions in which strong scintillations are more likely to occur. Scintillation is more likely to occur between sunset and after midnight local time during equinoctial months, with levels increasing with solar activity [2], [13], [29], [31], [35], [40].

Additional research can be found in the literature describing the dynamics of ionosphere and ionospheric scintillation supported by GNSS data (for example, see [17], [18], [24], [28], [30]).

Approaches designed to mitigate the ionospheric effects on precise GNSS positioning have been attempted previously by trying to model the higher order errors introduced by scintillation in upon the assumption that each satellite-receiver link is individually affected by scintillation. For those affected links, for example, different weights can be assigned to their range observables providing a more realistic stochastic model for the least squares adjustment applied in position computation [1]. In the case of range observables weights, a model describing the increase in phase tracking error in the presence of scintillation in a statistical stationary sense was utilised. With such an approach an average relationship between scintillation indices and guessed receiver properties was used to obtain the tracking error variance at an output of Phase Locked Loop (PLL) and Delay Locked Loop (DLL) of the GNSS receiver [8]. This variance can be applied in different positioning methods such as RTK and PPP to assign weights for each link [1], [9], [34].

Another approach was described by [47], which consists of an iterative Kalman filter designed to improve the PPP performance. Differential code biases are used for preliminary data quality checking, and data might be rejected before entering the filter estimation. In addition, thresholds in the cycle slip detection process are set with more flexibility during unexpected ionospheric conditions, decreasing the number

of false positive cycle slips and consequently reducing the number of re-initializations of ambiguity parameters. In principle, any approach designed to observables data editing and quality control can provide a countermeasure to deal with scintillation, based on the principle to exclude any subset of affected observables. Moreover, in this case, the amount of available data is reduced. The effectiveness of such approaches is restricted to the amount and the importance of any excluded observables in relation to the overall geometry. Data exclusion approaches are not considered in the scope of this paper because our intention is to model the scintillation effects considering all observables tracked by the receiver, therefore allowing to preserve original geometry and data.

In this work, we introduce a novel and alternative approach for the mitigation of increased PPP errors during scintillation that implements a correction to these errors on an epoch-by-epoch basis instead of a correction based on the statistics of these errors. Such a novel approach utilises all the data available from the receiver's processing chain (e.g. 50-Hz PLL I/Q samples and carrier phases) through which the link between scintillation and higher-order errors on the observables is established. This new approach can be summarised in three steps. The first step consists of a novel functional model to correct range errors in the observables, in which new terms on the observation equations were introduced to model the scintillation error in both code pseudorange and carrier phase measurements by using 50-Hz data. The second is a modified stochastic model that assumes different precisions in the observables by utilising the corrections arising from the first step. Finally, the third step is a strategy to attenuate the effects of losses of lock (i.e. data gaps) and, consequently, ambiguity re-initializations.

The assessment of our approach was conducted by processing a 30-day dataset (static data collected at Sao Jose dos Campos, state of Sao Paulo, Brazilian southeast region during high scintillation activity) with PPP. The overall results indicate a significant improvement in PPP accuracy. In some cases, our approach was completely able to recover the high-accuracy demanded on PPP applications by reducing the errors from meter to few decimeter level. Whilst only using 50-Hz scintillation data output from the receiver PLL at this stage, it is recognized that our approach could be generalised to include high rate data from both DLL and PLL and using a receiver designed to be free of losses of lock (and data gaps), e.g. GISMO [39].

A. Scintillation Monitor and Data Used

The study described here is supported by experimental data available at the UNESP network of ionospheric scintillation monitors http://is-cigala-calibra.fct.unesp.br based on Septentrio PolaRxS receivers. Such receivers are setup to output 50 Hz phase and amplitude samples for all visible satellites, with capabilities to track the main constellations and associated frequency bands [37]. At the time of submitting this paper, 11 monitoring stations collect data covering different geographical locations in Brazil. Most of the receivers have been collecting data since 2011. Therefore, the available data covers the ascension, peak and decay of the solar cycle no. 24 [43].

The work presented in this paper relies on dual-frequency GPS data (tracked on L1 and L2 frequencies). High-rate data (50 Hz) are available only at the output of the PLL for civil signals, that is, L1 C/A and L2C code. As a consequence, statistics based on high-rate data on L2-band are available only for satellites providing the L2 civil signal, i.e. currently the ones from the blocks IIR-M and II-F [10]. The high-rate data comprises in-phase/quadrature-phase correlated samples (hereafter denoted I_{corr} and Q_{corr}, respectively) and high-rate carrier phases ($\phi_{L1(C/A)}$ and ϕ_{L2C}, respectively, in units of cycles). Other observables, such as code pseudoranges and carrier phases from L2P ($\phi_{L2/P(Y)}$) or signal-to-noise ratio (SNR) are also available, but with lower sampling rates starting from 1s. In the RINEX v.2.11 specification, there is a single notation for the carrier phases at L2 whereas carrier phase measurements at L2 can be originated either from P(Y) or L2C codes in the PolaRxS receiver; extra care is required during data conversion tasks [3]. The RINEX v.3.03 standard was used in order to avoid confusion on the carrier phase measurements.

With the I_{corr} and Q_{corr} data, one can estimate the signal amplitude $r = \sqrt{I_{corr}^2 + Q_{corr}^2}$ and the signal intensity $I = |r|^2$ [44]. The scintillation indices are sampled at one-minute intervals. The S_4 has been the main statistic for indicating the severity of the amplitude scintillations. It is defined as the variance of the normalized signal intensity, as defined by [6]:

$$S_4 = \sqrt{\frac{\langle I^2 \rangle - \langle I \rangle^2}{\langle I \rangle^2}} \tag{1}$$

The brackets denote ensemble average. However, the time average over one-minute interval has been used as a common standard in commercial receivers [42], assuming ergodicity over 60s. With the high-rate phase observables, one can estimate the Sigma-phi ($\sigma_{\Delta\phi}$) index, defined as the standard deviation of the detrended carrier phase. The detrending process is usually performed by a 6th-order high-pass Butterworth filter with a cutoff frequency of 0.1 Hz (Van Dierendonck et al. 1993). The 60s interval has been also the main period to characterize the phase scintillation index (here referred to as $\sigma_{\Delta\phi,60}$).

The dataset selected for our experiments consists of a period of 30 days of static data collected during night time by the GNSS receiver located in Sao Jose dos Campos/Brazil (SJCU station, geographic coordinates: 23.2 S, 45.9 W, dip latitude: 17.5 S). The period considered is November, 2014, in which strong scintillation was observed. Time windows with duration of 2 hour each were selected for each day in the period of 22:00-24:00 (UT, or 19:00-21:00 in the local time). These time windows were selected mainly for two reasons. Firstly, because this time interval covers, in most cases, very low scintillation followed by significant higher levels affecting one or more satellites simultaneously. Secondly, because during these time windows, typically 5-7 satellites from blocks IIR-M and II-F were tracked simultaneously by the receiver above

an elevation angle of 10 degrees, therefore, providing enough satellite data coverage available to perform tests with PPP in the presence of scintillation.

B. The Effects of Ionospheric Scintillation on the GNSS observables

The effects of ionospheric scintillations on GNSS range observables (and consequently in position estimates) are correlated to the tracking ability of the receiver. Some of these effects can be sensitive to internal parameters in the GNSS receiver (see [11]) and can be summarised with losses of lock and degradation in the code and phase pseudorange measurements [47]. A loss of lock occurs when the receiver completely loses the track of a satellite. In such case, reacquisition of the signal from that satellite is required and a lack of observations will remain until the reacquisition process is completed [23]. Data gaps of a few tens of milliseconds can be typical in the presence of low-latitudes scintillation. On the other hand, moderate to strong scintillation originates higher-order errors in the observables (degrading their accuracy) in virtue of increased errors in the signal tracking and causing cycle slips [11].

In the applied dataset, data gaps occurred due to additional reasons as well. First, it can be noticed that PolaRxS receivers contain a setting by which a threshold to the C/No to be recorded can be applied. In such case, the receiver can be configured to disregard observables below a given C/No threshold, such as 15 dB. If the signal intensity drops below this user defined threshold, the observables are likely to not be included in the output observations file, therefore resulting in data gaps. Eventually, this threshold can be too conservative resulting in unnecessary data gaps [41]. In the dataset applied in this paper, the C/No threshold was set up to 25 dB which can be considered a suitable value to our context.

Second, data gaps can also be associated to half-cycle ambiguity. In our dataset, only phase observables with a full ambiguity were encoded in the RINEX files (assuming the standard configuration for the PolaRxS receiver). The observables flagged with half-cycle ambiguity are discarded during RINEX encoding with the manufacturer's data convert utility. As L2C signal has a pilot component which is designed to be tracked with full-cycle ambiguities, the ϕ_{L2C} is not affected by half-cycle ambiguity (private communication from Septentrio's Support Team). On the other hand, there are several cases in which the half-cycle ambiguity strongly affects the availability of $\phi_{L1(C/A)}$ during scintillations (as it will be shown in Fig. 1). The presence of consecutive data gaps in cases where the receiver keeps lock of satellite may induce cycle slip detection algorithms to falsely identify a cycle slip occurrence possibly causing unnecessary re-initialization of the ambiguity parameter [47].

Fig. 1 illustrates examples of data gaps for four minutes of $\phi_{L1(C/A)}$ data tracked by the SJCU station for the PRN24 in the night time of November 05, 2014. In the top plot (Fig. 1a), the high-rate signal intensity is shown (in units of dB). In the bottom plot, the high-rate detrended carrier phase is shown (in units of cycles). The grey and red dots indicate whether the

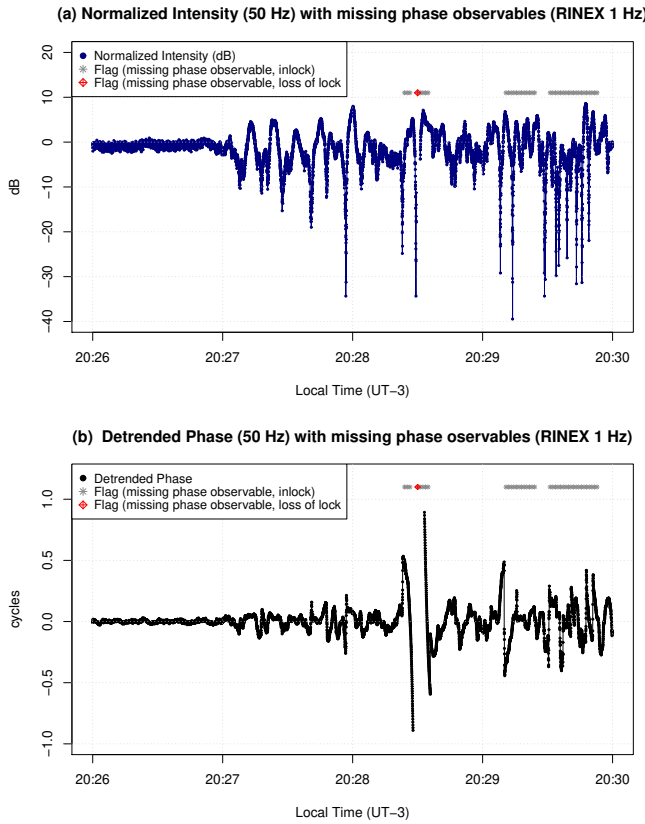

Fig. 1. The top plot (a) shows the normalized intensity over a period of 4 minutes in blue; the grey dots indicate whether the phase observable was not included in the respective RINEX file due to half-cycle ambiguity and the red dot indicates whether a loss of lock occurred. The bottom plot (b) shows the detrended carrier phase in black over the same period; the grey and red dots have the same meaning as in the top plot. Intensity and phase data tracked by the SJCU receiver for the PRN24 in the night time of November 05, 2014.

phase observables are missing in the corresponding RINEX file (RINEX data have a sample rate of 1s). A case in which the receiver completely loses the track of the satellite can be identified between 20:28 and 20:29 LT. When a loss of lock occurs, no output is available from the receiver until the reacquisition of the respective signal is completed (red dot). Several cases in which the observables are missing due to half-cycle ambiguities can also be inferred (indicated with grey dots). Cases in which the output carrier phase has degradation in accuracy can be inferred by the increase in the detrended carrier phase variation (Fig. 1b), as after 20:27 (LT).

Losses of lock imply reduced number of observations (i.e. data gaps) and therefore deterioration of geometry. Degradations in accuracy of observables, if not properly modelled, can affect any positioning method as they affect the range measurements that are the basis of the position determination. Data gaps cause different availability for observables tracked under different frequencies. As a consequence, they can be more sensitive for linear combinations between observables, like double differences, iono-free (IF) and code smoothed by phase.

Another aspect is the detection and/or repair of cycle slips which can be either sensitive to losses of lock, range degradations, and data gaps [47]. How these scintillation-

induced effects on the observables will affect the positioning performance from the user's perspective will not only depend on the relation between satellite geometry and affected links, but also on how well the observables are modelled taking these effects into account.

II. Functional and Stochastic Models in Standard PPP

In this work the PPP approach [48] based on the in-house RT-PPP software [25] was applied for processing data. The PPP approach was chosen due to its feature to reach high accuracy level with a single receiver (absolute positioning, no baseline is required). The RT-PPP software was chosen due to its flexibility of configurations, as well as a special feature to allow the application of possible scintillation mitigation approaches. RT-PPP can read an external input file with variances of GPS observables for every epoch, therefore allowing to evaluate different stochastic modelling of observables. Also, the RT-PPP provides the background of a well consolidated PPP online service available at UNESP (available at http://is-cigala-calibra.fct.unesp.br/ppp/) and has been used on several investigations related to PPP at the literature, such as in [9], [26], [36].

A. Functional Model in Standard PPP

Different configurations can be applied when processing data with PPP approach, such as the observables selection [16], products (such as satellites orbits and clock corrections), strategies for correcting the main errors, such as ionospheric/tropospheric refractions, ambiguity resolution [7], outlier detection and quality control [21], [22], [46], among others. Traditionally, PPP based on iono-free linear combination (i.e. with code and phase observables), is described on the basis of errors that do not encompass scintillation, as follows. The observation equation for undifferenced code pseudorange (in units of meters) between satellite s and receiver r at the frequency $Li = L1, L2$, at a given epoch t, can be expressed as [19], [25], [27]:

$$PR^s_{rLi}(t) = \rho^s_r(t) + c[dt_r(t) - dt^s(t)] + I^s_{rLi}(t) + T^s_r(t) + \varepsilon_{PR^s_{rLi}} \quad (2)$$

where ρ^s_r is the geometric range, c is the propagation velocity (assumed to be the speed of light in free space), dt_r is the receiver clock error, dt^s is the satellite clock error, I^s_{rLi} is the ionospheric delay given frequency Li, T^s_r is the tropospheric delay and the term $\varepsilon_{PR^s_{rLi}}$ denotes negligible and non-modelled errors (including noise). For the undifferenced carrier phases, the observation equations (in units of meters) can be written as:

$$\lambda_{L_i}\phi_{L_i r}{}^s(t) = \rho^s_r(t) + c[dt_r(t) - dt^s(t)] - I^s_{rLi}(t) + T^s_r(t) + \lambda_{Li}N_i + \varepsilon_{\phi^s_{rLi}} \quad (3)$$

where λ_{Li} denotes the carrier respective wavelength, N_i is the ambiguity of the carrier phase and the other terms are similar to those ones presented in (2). The iono-free linear combination with L1 and L2 data can be used for eliminating the first order effects of the ionospheric refraction. In such case, for both code and phase pseudoranges, the L1-L2 equations are combined by applying specific coefficients based on the ratio of their frequencies [15], [27]:

$$PR^s_{rIF}(t) = (m_1)PR^s_{rL1}(t) + (m_2)PR^s_{rL2}(t) \quad (4)$$

$$\lambda_{IF}\phi^s_{rIF}(t) = (m'_1)\phi^s_{rL1}(t) + (m'_2)\phi^s_{rL2}(t) \quad (5)$$

where:

$$m_1 = m'_1 = f_1^2/(f_1^2 - f_2^2) \cong 2.5457 \quad (6)$$

$$m_2 = -f_2^2/(f_1^2 - f_2^2) \cong -1.5457 \quad (7)$$

$$m'_2 = -f_1 f_2/(f_1^2 - f_2^2) \cong -1.9837 \quad (8)$$

Finally, the functional model of the iono-free linear combination can be expressed as:

$$PR^s_{rIF}(t) = \rho^s_r(t) + c[dt_r(t) - dt^s(t)] + T^s_r(t) + \varepsilon_{PR^s_{rIF}} \quad (9)$$

$$\lambda_{IF}\phi^s_{rIF}(t) = \rho^s_r(t) + c[dt_r(t) - dt^s(t)] + T^s_r(t) + \lambda_{IF}N_{IF} + \varepsilon_{\phi^s_{rIF}} \quad (10)$$

The above steps summarise the functional model of the standard (with no mitigation for scintillation) PPP that forms the basis for the comparative tests in this paper. Under this description any residual error arising because of scintillation (at low and high latitudes) is forced into the last generic error term ($\varepsilon_{PR^s_{rIF}}$ and $\varepsilon_{\phi^s_{rIF}}$) that is typically modelled on a statistical basis. A more precise characterisation of scintillation-induced errors is necessary in order to improve PPP performance in the presence of ionospheric scintillation.

B. Stochastic Models in Standard PPP

The residual errors in (9)-(10) ($\varepsilon_{PR^s_{rLi}}$ and $\varepsilon_{\phi^s_{rLi}}$) are modelled further in a stochastic sense, by modelling their standard deviations. The stochastic model of GNSS observables in the least squares adjustment is usually based either on constant variances for each type of observable (σ^2_{obs}) or assuming variances being scaled as a function of satellite elevation angles ($\sigma^2_{obs,Elev}$). In the RT-PPP software (with no scintillation correction) the default constant standard deviation of undifferenced observables (σ_{obs}) can be adopted with values that will be later propagated in the iono-free combination. The following values were applied for the phase and code observables: $\sigma_{PR_{L1}} = 0.8$; $\sigma_{PR_{L2}} = 1.0$; $\sigma_{\phi_{L1}} = 0.008$ and $\sigma_{\phi_{L2}} = 0.010$, in units of meters. The stochastic model can be related to the elevation angle through the following relation [38]:

$$\sigma^2_{obs,Elev} = \frac{1}{\sin(Elev)}\sigma^2_{obs} \quad (11)$$

C. Stochastic Models for Scintillation used in Previous Approaches

The modelling of the scintillation contribution to the residual errors ($\varepsilon_{PR^s_{rLi}}$ and $\varepsilon_{\phi^s_{rLi}}$) in (9)-(10) was attempted by relating them to tracking error variances. According to this strategy, the tracking error variance can be related to the scintillation index under the assumption of a standard linearised loop. Here, we notice that in doing so, an underlying assumption of ergodic processes (for residual errors and scintillation) has to be made. A tracking error model can be used to relate different signal metrics (such as scintillation indexes) and/or receiver and signal properties for estimating the predicted tracking error variance (also referred to as tracking jitter) with the output of the PLL and DLL of GNSS receivers. The tracking jitter models proposed by Conker *et al.* [8] were applied for example in [1] to provide weights for the observables as input to stochastic model in positioning estimation. According to the Conker model, the tracking jitter variance ($\sigma^2_{\phi\varepsilon}$) of the PLL of GPS receivers can be expressed by three components:

$$\sigma^2_{\phi\varepsilon} = \sigma^2_{\phi S} + \sigma^2_{\phi T} + \sigma^2_{\phi Osc} \tag{12}$$

where $\sigma^2_{\phi S}$ is the scintillation error component, $\sigma^2_{\phi T}$ is the thermal noise component, $\sigma^2_{\phi Osc}$ is the oscillator noise component. The tracking jitter variance at output of DLL is expressed only by the thermal noise component ($\sigma^2_{PR\varepsilon} = \sigma^2_{PR_T}$). In summary, the Conker models provide variances for the following observables $\sigma^2_{\phi\varepsilon L1(C/A)}$, $\sigma^2_{\phi\varepsilon L2/P(Y)}$, $\sigma^2_{PR\varepsilon L1(C/A)}$ and $\sigma^2_{PR\varepsilon L2/P(Y)}$, and take as input parameters such as the S_4 index, the spectral strength of the phase scintillation power spectral density (PSD) at 1 Hz (T), the spectral slope (p), receivers loop natural frequencies and order of both PLL and DLL tracking loops, chip lengths of the code observables, etc.

Possible limitations of the Conker model has been highlighted at the literature, mainly if the intention is to use the output from the model for de-weighting GPS observables in positioning. The Conker model is valid only for $S_4 < 0.707$. From this threshold, a loss of lock is assumed and no output would be necessary from the model. Nevertheless, receivers can be able to keep the lock even above this S_4 threshold value. In such cases, no output is available from the model then resulting in missing variance values. Another limitation is related to the model's output sample rate. Although not clearly stated, the statistical interval of 60 s is inferred from the Conker model equations, as they use the S_4 index as input (as well as spectral parameters). As a consequence, a reshape approach is necessary for making the outputs compatible with different sample rates applied in positioning, such as 1 s or 15 s. These limitations are discussed in [34] where few modifications were proposed to overcome them. Another possible limitation regarding the Conker model is the assumption of the Nakagami-m distribution for the amplitude scintillations. As demonstrated by [33], the α-μ distribution [45] outperforms other statistical distributions previously used to describe amplitude scintillations, including the Nakagami-m distribution. By assuming the α-μ statistical distribution, the two parameters α and μ are used to describe the scintillation, in contrast of the single value of S_4 index in Nakagami-m case. Such an aspect can imply in advantages for describing scintillation effects on GPS observables, because the S_4 index by itself cannot be considered a proper indication of ionospheric degradation at some cases, as during strong scintillations periods [20], [32]. The Conker model was rewritten taking the α-μ coefficients and assuming correlation between phase and amplitude scintillations in [32]. Another possible limitation about these tracking error models is regarding the observables. The Conker and later modifications relies on semi-codeless tracking (L2 carrier aided by L1 PLL). In contrast, there is no high-rate output from the PolaRxS for semi-codeless tracking. Such aspect is considered in [9], where a tracking error model based on high-rate data were developed for L1 and its application for semi-codeless receiver depends on application of scaling factors between L1 and L2.

The variance provided by such models can be applied to the stochastic model of any positioning approach, such as PPP and RTK, therefore constituting a scintillation mitigation approach. This approach seems to show some improvement when compared to the standard one, however, the improvement seems to not be good enough to supply high-accuracy applications, especially during strong scintillations. The limitation with these approaches is due to the assumption of ergodicity of scintillation (for example, over an entire minute). For example, the periods of fading typically observed during low-latitudes scintillation are up to few seconds: a correction based on standard deviations over a given time window is likely to under/overestimate the real error induced by scintillation.

III. Our approach

The motivation of the novel approach proposed here is to provide a reliable correction for the scintillation contribution to scintillation-induced errors such that PPP can be used consistently even during scintillation events. Our approach consists of three steps: **a)** a new functional model to correct range errors in the code and phase pseudorange observables; **b)** a new stochastic model that uses the same errors estimated at step a to provide a more realistic scenario for the least squares adjustment and mitigate remaining errors in the ranging observables; and **c)** a strategy to attenuate the effects of losses of lock and consequently ambiguity re-initializations. These strategies are detailed hereafter.

A. Step a – New Functional Model

Contrary to previous approaches, the correction for scintillation-induced higher order errors is made here on an epoch-by-epoch basis rather than on a stochastic sense (i.e. not only through the use of variances associated with scintillation). The contribution of scintillation-induced signal perturbations on the observables can be indeed described as follows. The undifferenced observables (in units of meters) from (2) and (3), respectively, are rewritten as:

$$\begin{aligned} PR^s_{rLi}(t) = \rho^s_r(t) + c[dt_r(t) - dt^s(t)] + I^s_{rLi}(t) + \\ T^s_r(t) + dScint_{PR^s_{rLi}}(t) + \varepsilon_{PR^s_{rLi}} \end{aligned} \tag{13}$$

$$\lambda_{L_i}\phi_{L_i r}^{s}(t) = \rho_r^s(t) + c[dt_r(t) - dt^s(t)] - I_{rLi}^s(t) + T_r^s(t) + \lambda_{Li}N_i + \lambda_{Li}dScint_{\phi_{rLi}^s}(t) + \varepsilon_{\phi_{rLi}^s} \quad (14)$$

where the new terms $dScint_{PR_{rLi}^s}(t)$ (in units of meters) and $dScint_{\phi_{rLi}^s}(t)$ (in units of cycles) represent, respectively, the errors induced by ionospheric scintillation in the code and phase observables at frequency Li.

The term $dScint$ is not directly and easily scalable according to the respective observable and, hence, does not necessarily cancel out from ionosphere-free combination. Therefore, the iono-free code and phase observables can be rewritten as:

$$PR_{rIF}^s(t) = \rho_r^s(t) + c[dt_r(t) - dt^s(t)] + T_r^s(t) + dScint_{PR_{rIF}^s}(t) + \varepsilon_{PR_{rIF}^s} \quad (15)$$

$$\lambda_{IF}\phi_{rIF}^s(t) = \rho_r^s(t) + c[dt_r(t) - dt^s(t)] + T_r^s(t) + \lambda_{IF}N_{IF} + \lambda_{IF}dScint_{\phi_{rIF}^s}(t) + \varepsilon_{\phi_{rIF}^s} \quad (16)$$

where the same iono-free coefficients are applied to the respective $dScint$ terms. It is to be noticed that (15)-(16) depend upon t: that is, an epoch-by-epoch correction for the error terms $dScint$ can be sought for residual errors on observables induced by scintillation. It is worth noticing that as the ambiguity resolution could be, in principle, limited in the presence of scintillation, one can infer that the errors $dScint_{\phi IF}$ and N_{IF} are also related. Furthermore, the term $dScint_{\phi IF}$ is expected to be larger in the equatorial anomaly region (and in polar and auroral regions) with moderate to strong scintillations.

The scintillation term is related to the receiver's architecture. In particular, one can tune the settings to increase robustness against scintillation by widening the tracking bandwidth, for example [11]. The effect of widening the tracking bandwidth can be understood in terms of the comparison between $dScint_{\phi_{rIF}^s}$ and $\varepsilon_{\phi_{rIF}^s}$ in the iono-free combination. Widening the tracking bandwidth on L1, L2 or both would produce noisier observations of the carrier phases, hence $\varepsilon_{\phi_{rIF}^s}$ would increase. In this case, if the bandwidth widening leads to the condition $dScint_{\phi_{rIF}^s} \ll \varepsilon_{\phi_{rIF}^s}$ then the observables and the iono-free combinations would only be affected by measurement noise (thermal noise), removing the behavior which maximises the residuals around the anomaly peaks and at auroral/polar latitudes. However, this operation would result in an overall enhancement of the noise level, thus affecting the accuracy of precise positioning because of possible degradation in the phase pseudoranges.

Due to the nature of ionospheric irregularities, large-to-small scales ionisation gradients contribute to the scintillation-induced error term. The contribution consists of two components: slower total electron content (TEC) temporal fluctuations and faster scintillation fluctuations in the carrier phases. These two components have typical time scales ranging from several seconds to under a second. Hence, fast sampling of received signals is necessary in order to appreciate the fluctuations of these two components.

In the present work, the process to estimate the scintillation-induced error term on the carrier phase observable at frequency Li ($dScint_{\phi_{Li}}$) was performed by describing it according to its two components: i.e. a high-frequency component (labelled as $dScint_{\phi_{Li}}^{HF}$) to account for faster scintillation fluctuations on the carrier phase and a low-frequency component (labelled as $dScint_{\phi_{Li}}^{LF}$) to account for slower TEC temporal fluctuations:

$$dScint_{\phi_{Li}} = dScint_{\phi_{Li}}^{HF} + dScint_{\phi_{Li}}^{LF} \quad (17)$$

Both $dScint_{\phi_{L1(C/A)}}$ and $dScint_{\phi_{L2C}}$ were estimated from high-rate (50 Hz) amplitude and phase data provided by PolaRxS receiver. In this step, the L1 and L2 carrier phases were individually detrended by applying a sixth order Butterworth filter with a cut-off frequency of 0.1 Hz. The $dScint_{\phi_{Li}}^{HF}$ is the high-pass component of the detrended carrier phase and $dScint_{\phi_{Li}}^{LF}$ is the low-pass component [12], [42].

After estimating $dScint_{\phi_{Li}}$ for each carrier frequency (17), the corresponding scintillation-induced error term considering the iono-free combination can be finally obtained as:

$$dScint_{\phi_{rIF}^s}(t) = (m_1')dScint_{\phi_{rL1}^s}(t) + (m_2')dScint_{\phi_{rL2}^s}(t) \quad (18)$$

Accordingly, it is:

$$dScint_{\phi_{rIF}^s}^{HF}(t) = (m_1')dScint_{\phi_{rL1}^s}^{HF}(t) + (m_2')dScint_{\phi_{rL2}^s}^{HF}(t) \quad (19)$$

$$dScint_{\phi_{rIF}^s}^{LF}(t) = (m_1')dScint_{\phi_{rL1}^s}^{LF}(t) + (m_2')dScint_{\phi_{rL2}^s}^{LF}(t) \quad (20)$$

This way, the low and high frequency components of the scintillation-induced error term can be estimated by using information available from 50-Hz data present in any receiver processing chain.

The term $dScint_{\phi_{Li}}$ depends upon TEC fluctuations (low-frequency component) and scintillation (high-frequency component). TEC temporal fluctuations are associated with ionospheric scintillation because ray paths traverse large-to-small scale gradients in plasma density. At low latitudes, a cut-off frequency value of 0.1 Hz has been consolidated after many years of measurements of ionospheric scintillation on GPS signals.

The overall variance described by $dScint_{\phi_{Li}}$ does not depend upon the cut-off frequency but from the specific ionospheric propagation conditions: this is the only surviving term in the iono-free combination. The component $dScint_{\phi_{Li}}^{LF}$ describes all TEC fluctuations occurring over frequencies between the satellite motion and 0.1 Hz (large-to-medium scale plasma gradients), while $dScint_{\phi_{Li}}^{HF}$ describes all scintillation-induced fluctuations between 0.1 Hz to the 25-Hz Nyquist limit (small-scale plasma gradients).

The cut-off frequency of 0.1 Hz is purely utilised to separate $dScint_{\phi_{Li}}$ in two different components. This allows to model residuals induced by scintillation over different time scales.

Of course, the choice of a different detrending cut-off would imply the estimation of the components $dScint_{\phi_{Li}}^{LF}$ and $dScint_{\phi_{Li}}^{HF}$ to vary, however, the overall term $dScint_{\phi_{Li}}$ (i.e. all the residuals induced by large-to-small scale phase fluctuations) would remain the same.

At high latitudes, for example, a different choice of the detrending cut-off frequency can be made owing to different ionospheric propagation conditions, where faster TEC phase

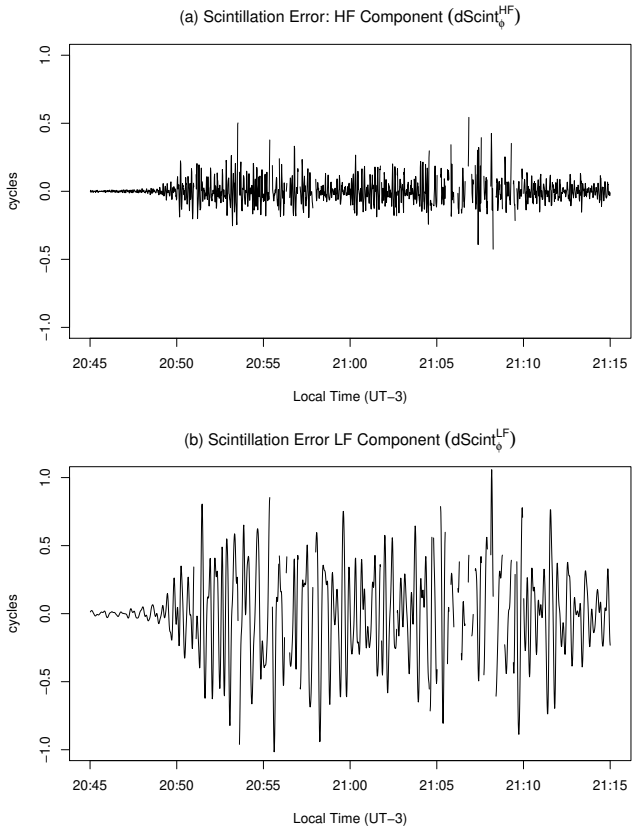

Fig. 2. The top (a) and bottom (b) plots show, respectively, the high-frequency (HF) and the low-frequency (LF) components of scintillation-induced error tracked by PRN 25 in the night-time of DOY 307/2014.

fluctuations can be present. For more details about this, please refer to the discussion contained in [12].

Examples of the estimation of both low-frequency and high-frequency of the scintillation-induced error term $dScint_{\phi_{Li}}$ can be seen in Fig. 2. The plots show the $dScint_{\phi_{Li}}^{HF}$ and $dScint_{\phi_{Li}}^{LF}$ components estimated from real data tracked (PRN 25) by SJCU receiver in the nigh-time of November 3, 2014 (DOY 307/2014). One can see that the high-frequency term presents rapid fluctuations associated with scintillation, while the low frequency component shows slower trends associated with TEC temporal fluctuations.

It is reasonable to expect different behaviours for the high-frequency and low-frequency components at high latitudes (this point is, however, beyond the scope of the present work). The carrier phase observables corrected from scintillation-induced errors (ϕ'_{Li}, in units of cycles) is obtained as:

$$\phi'_{Li} = \phi_{Li} - dScint_{\phi_{Li}} \tag{21}$$

where both ϕ_{Li} and $dScint_{\phi_{Li}}$ are sampled at 50 Hz. The same method can be used to model the scintillation-induced error component for code pseudoranges ($dScint_{PR_{Li}}$). This was not possible in the present work due to the lack of similar high-rate data at the DLL output of the PolaRxS receiver. However, the method can be easily generalised to model the $dScint_{PR_{Li}}$ error term as well.

B. Step b – Modified Stochastic Model

Two remaining aspects need to be tackled next: (i) the fact that the error terms $dScint_{\phi IF}$ and N_{IF} are related and (ii) the fact that the error term $dScint_{PR_{Li}}$ in (15) could not be modelled for pseudoranges due to the lack of relevant data output from the scintillation monitor utilised. The PolaRxS monitor indeed outputs high-rate samples for carrier phases and signal levels as deduced from its PLL; no similar high-rate samples were available for the pseudoranges in our dataset.

Hence, after step a some residual errors in the presence of scintillation can still remain. In order to overcome this aspect, and without a precise knowledge of the algorithms specifically implemented in the PolaRxS receiver, a stochastic correction of these residual errors is proposed on the basis of a corresponding standard deviation for the carrier phase observables. Incidentally, if the tracking algorithms implemented in a receiver were precisely known, then step b could be replaced by an epoch-by-epoch correction following the same strategy as in step a.

Our modified stochastic model follows the general concept of assigning different weights for each of the GNSS observables at every satellite-receiver link, where the weight is defined through the standard deviation of the observables, as proposed by [1]. The weights are then applied in the RT-PPP software during the least squares adjustment.

Here, instead of assigning weights in an arbitrary fashion, we propose the use of the scintillation-induced error terms to calculate satellite-specific weights at each epoch for the carrier phase observables. The methodology can be summarised as follows. Due to the lack of relevant output data from the PolaRxS DLL section, the scintillation-induced error for code pseudoranges ($dScint_{PR_{Li}}$) was described through constant standard deviations ($\sigma_{PRL1(C/A)} = 0.80$ m and $\sigma_{PRL2C} = 1.0$ m). On the other hand, in the case of the carrier phase observables $\phi_{L1(C/A)}$ and ϕ_{L2C}, a satellite-specific weight can be calculated by using the following empirical relationship:

$$\sigma^2_{\phi_{Li},dScint}(t) = \left(1 + \kappa|\lambda_i dScint_{\phi_{Li}}(t)|^y\right)^2 \cdot \sigma^2_{\phi_{Li}} \tag{22}$$

that relates the measured scintillation-induced error terms $dScint_{\phi_{L1(C/A)}}$ and $dScint_{\phi_{L2C}}$ with the nominal standard deviations $\sigma_{\phi L1(C/A)}$ and $\sigma_{\phi L2C}$, respectively, over a time interval of 1 second.

In (22), the scaling parameter κ has dimensions of $[m^{-y}]$. The functional form of (22) was derived empirically as a best fit to the observations collected through the PolaRxS scintillation monitor. The scaling factor κ represents the magnitude of the remaining range errors in the phase observables after correction from step a and y is an exponential factor that represents the saturation level of the absolute error due to scintillation on the carrier phase observable (dScint$_{\phi_{Li}}$).

Here, the values of $\kappa = 35$ and $y = 0.5$ were empirically deduced through a best fit to the raw data and they were utilised in equation (22) for both L1 and L2 carrier phase observables measured in the dataset considered.

Equation (22) can be seen as a mapping function that relates the nominal standard deviation corresponding to these phase

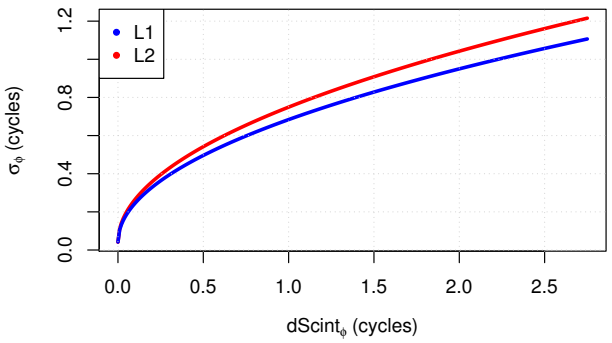

Fig. 3. Standard deviation of the phase observables for different scintillation-induced error values, for both L1 and L2 carriers.

observables and the expected scintillation-induced residual error term. The novelty of the relationship in (22) is the fact that the correcting standard deviation is now specified at each epoch (rather than through an arbitrarily constant value). This allows the estimate of a correction that can be implemented on an epoch-by-epoch basis.

Fig. 3 illustrates the relationship described by (22) between the $dScint_{\phi Li}$ and the respective estimated standard deviations ($\sigma_{\phi Li}$). The default values for the nominal standard deviations $\sigma_{\phi L1(C/A)} = 0.008$ m and $\sigma_{\phi L2C} = 0.01$ m are considered in the case of no scintillation ($dScint_{\phi_{Li}} = 0$).

C. Step c – Strategy to minimize effects of losses of lock

Several losses of lock occurred in the data associated to strong ionospheric scintillations. In addition, data gaps mainly due to half-cycle ambiguity at $\phi_{L1(C/A)}$ were often observed during deep fadings in intensity. In the experiments carried out in this paper, the RT-PPP software was used to assess the performance of our proposed method on PPP. The RT-PPP uses the algorithm designed by [4] to detect cycle slip occurrence. If a cycle slip is detected, the respective ambiguity parameter for that satellite is re-initialized [25], [26]. As no modifications were made to the PPP software for performing our tests, we couldn't use the [47] approach to set up the thresholds more flexibly during scintillations. However it can be done in the future.

As a consequence of successive losses of lock, the $dScint_{\phi Li}$ can be missed during few epochs until the reacquisition process is completed to ensure reliability of the estimated corrections. During our tests, observables were not excluded from input RINEX file for performing PPP. There are cases in which the phase observable can be present but $dScint_{\phi Li}$ could not be computed due to data gaps. For such cases, we devised a complementary further step that consists in a time window-based function assigning variances when $dScint_{\phi Li}$ is unavailable because of data gaps. Given any epoch t, the strategy consists in calculating an upper bound for the variance for the given phase observable if a loss of lock has occurred in a neighborhood $[t-w, t+w]$, where w is a time period (in seconds) empirically defined in which the signal might be overloaded by scintillation errors. We apply the maximum feasible value for the $dScint_{\phi}$ in (22) for estimating the variance to these epochs. As demonstrated in [11], cycle slips can be more susceptible to occur during the reacquisition period. Therefore, providing such time window based overestimation in the variances of the affected observables reduces the impact of the sudden change in geometry due to the losses of lock and reduces the effects of range degradations due to possible cycle slips during the reacquisition period. Equation (22) can be rewritten in terms of the following conditional relation:

$$\sigma^2_{\phi_{Li},dScint}(t) = \begin{cases} \left(1+\kappa|\lambda_i dScint_{\phi_{Li}}(t)|^y\right)^2 \cdot \sigma^2_{\phi_{Li}}, & \text{inlock in [t-w,t+w]} \\ \left(1+\kappa|\lambda_i 2.6|^y\right)^2 \cdot \sigma^2_{\phi_{Li}}, & \text{loss of lock in [t-w,t+w]} \end{cases} \quad (23)$$

In our tests, the upper bound was set given (22) and argument $dScint_{\phi Li} \approx 2.6$ cycles, because above this value (approximately) the receiver is likely to lose the lock. The time window $w = 60$ s was applied. These values were determined empirically from our dataset and depend on the relation between tracking ability of the receiver and the severity of the scintillations (as identified by relation between losses of lock occurrence and $dScint_{\phi Li}$). It can be noticed that (23) provided inputs for variances in cases when observables can be present in the RINEX file but $dScint_{\phi Li}$ could not be computed due to successive data gaps.

IV. The Performance of Our Approach to Mitigate for Scintillation in PPP

In order to assess the performance of our model in the GPS positioning, experimental data collected in November 2014 at Sao José dos Campos were processed with the RT-PPP software. The standard approach (the standard PPP without the scintillation correction) was compared with our proposed method within a dataset of 30 days processing each with a window of 2 hours duration (19:00-21:00 LT). The non-mitigated solution was based on default PPP functional model (9-10) and the elevation-based stochastic model (11). Our proposed mitigated solution was based on the modified versions of functional (15-16) and stochastic (23) models.

The same additional setup was applied on the RT-PPP software for both mitigated and non-mitigated solutions. The iono-free linear combination was applied for processing both code and phase pseudoranges at L1 and L2. Only the observables from civil codes were considered for performing the combination (namely, the pseudoranges $PR_{L1(C/A)}$ and PR_{L2C} and carrier phases $\phi_{L1(C/A)}$ and ϕ_{L2C}, extracted from RINEX v.3.0.3). Tropospheric refraction was corrected by the global model from European Centre for Medium-Range Weather Forecasts (ECMWF) and the Vienna Mapping Function (VMF) was applied [5]. Final orbit and clock products provided by the International GNSS Service (IGS) were utilised. Data were processed in kinematic mode, in which the coordinates are estimated every epoch, but the ambiguities of the iono-free linear combination are estimated in an accumulative way via recursive least squares adjustment. If a cycle slip is detected (via the algorithm presented in [4]), the ambiguity parameter is re-initialized [25], [26]. Additional default models/corrections available on RT-PPP were also applied, such as corrections

for receiver and satellite phase center variation (PCV), Earth Body Tides (EBT), Ocean Tides Loading (OTL), differential code biases (DCBs), phase windup and relativistic effects. With such configuration, accuracies in the few centimeter level are expected in the estimated position components after initialization convergence period (time interval required for the estimated position components converge few centimeter level) [14]. In absence of scintillation, this configuration lead to a convergence time ranging approximately between 10 and 20 minutes.

In this paper, the proposed approach could not be compared with the previous approaches attempted to mitigate scintillation in the positioning (described in Section II-C). The main reason is the lack of high-rate data at the output of L2/P(Y) in the applied PolaRxS receiver which limits the full implementation of models like Conker and later modifications [8], [32], [34]. Therefore, only L1(C/A) and L2C data were applied in our tests, comparing the standard PPP without the scintillation correction with our proposed method. Representative cases are illustrated in Figs. 4-5.

In Fig. 4 results for DOY 307/2014 are presented. The plots show the positioning errors at the North (DN), East (DE) and Up (DU) components epoch-by-epoch, for both standard PPP solution (top) and mitigated PPP solution (bottom), according to the proposed method. The red line indicates the number of satellites used at each epoch, and the black dots are flags to indicate whether a cycle slip was detected by the RT-PPP (and consequently, the ambiguity parameter was re-initialized). In this example, our mitigation approach was able to maintain the high-accuracy expected to be achieved with PPP even in the presence of strong scintillation. The standard-deviation of 3D-RMSE reduced from 0.54 m in the standard PPP to 0.11 m in our mitigated approach. A reduced number of satellites broadcasting the civil data were observed in that time periods (varying from 5 to 7 satellites), but still good results were achieved with PPP during absence of scintillations, therefore indicating the limited geometry did not affect the positioning accuracy. Such situation will improve in the future with more satellites providing L2C data.

Another example is presented in Fig. 5 for DOY 316/2014. The comparison shows the proposed mitigation approach significantly reduced the effect of ambiguities re-initialization due to cycle slips detection, reflecting in better positioning accuracy in horizontal and vertical components with improvements raising up to 76% when comparing to the standard solution.

Even with significant improvements in the overall assessment, there were cases in which our approach was unable to provide the high accuracy expected with PPP. One example is presented in the comparison of Fig. 6 showing the results for DOY 319/2014. In such day, our approach was able to reduce the magnitude of the errors in positioning domain after scintillations between 20:30 and 20:40 (approximately). Otherwise, the increase in successive losses of lock after 20:40 limited the improvement in positioning accuracy due to several re-initialization affecting more than one PRN simultaneously. This lead to a very harsh scenario limiting the improvements. With more modernized satellites, this situation is expected to improve. Some of the satellite ray paths are in a resonant

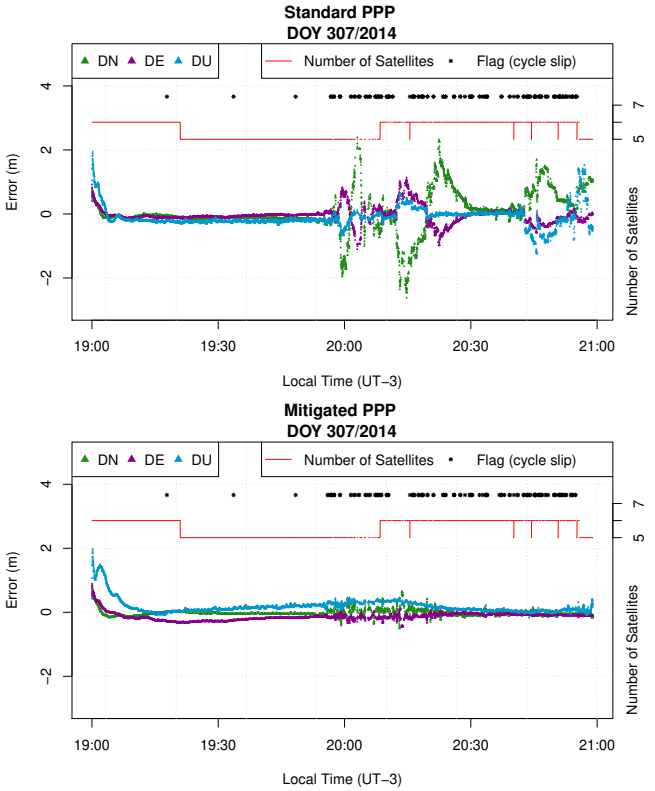

Fig. 4. Comparison between standard (non-mitigated) and mitigated solution for DOY 307/2014. The positional accuracy is presented by the North (DN), East (DE) and Up (DU) error components. The red line indicates the number of satellites and the black dots indicate whether a cycle slip (followed by ambiguity re-initialization) was detected by the PPP software.

condition, whereby they propagate between trains of plasma bubbles separated by a spatial distance that does not leave enough time for the mitigated PPP solution to converge.

A summary of comparative results between the non-mitigated solution and our proposed method is presented in Fig. 7. Plots show the standard deviation (top plot) and the average (bottom plot) of the 3D-RMSE for the kinematic PPP solution for each day during the 19:30-21:00 (LT) period. The period comprising the first 30 minutes of data where convergence takes place at each window, e.g., between 19:00 and 19:30, were not included in positioning accuracy evaluation in Fig. 7. Besides the error bars for the both solution types, the dashed lines indicate the number of cycle slip cases as detected by the RT-PPP software. Next to Fig. 7, Table I provides numerical details with additional quantities. The number of missing observables per type is presented, being distinguished between missing either due to loss of lock or half-cycle ambiguity. The number of $S_4 > 0.3$ cases are also presented for L1 and L2 (with an elevation cut-off of 10 degrees).

V. Discussion

Results indicate that most of the days with presence of strong scintillation were successfully mitigated, including days with several cycle slips and consequent ambiguities re-initializations carried out by RT-PPP Software. The improvements rate when comparing the non-mitigated PPP with our

TABLE I
SUMMARY OF THE CONDITIONS REGARDING OBSERVATIONS AND SCINTILLATIONS, COMPARISON BETWEEN NON-MITIGATED AND MITIGATED PPP.

DOY	No of. Missing Observables				Scintillation		Standard PPP			Mitigated PPP		
	Loss of Lock		Half-Cycle Ambiguities		No. of S_4>0.3		3D-RMSE (m)		No. of Cycle Slips	3D-RMSE (m)		No. of Cycle Slips
	L1	L2	L1	L2	L1	L2	Std. Dev.	Avg.		Std. Dev.	Avg.	
305	9	171	100	0	75	86	1,04	0,62	76	0,15	0,40	74
306	0	0	0	0	0	2	0,08	0,32	6	0,07	0,25	6
307	43	197	655	0	85	92	0,54	0,57	149	0,11	0,23	148
308	0	0	0	0	0	0	0,13	0,29	6	0,14	0,30	6
309	24	74	360	0	20	19	1,11	0,79	54	0,09	0,34	53
310	49	387	1463	0	217	264	1,08	1,03	246	0,51	0,60	215
311	17	18	259	0	49	53	0,70	0,96	24	0,49	0,63	25
312	0	10	88	0	33	37	0,22	0,48	14	0,41	0,36	13
313	8	18	625	0	87	90	0,59	0,94	37	0,46	0,64	33
314	0	0	0	0	0	0	0,15	0,24	5	0,29	0,37	6
315	30	111	235	0	122	131	1,15	1,34	89	0,23	0,72	64
316	15	46	272	0	88	91	0,94	1,34	42	0,19	0,37	40
317	13	47	484	0	136	147	2,30	2,14	67	0,83	0,71	52
318	0	0	0	0	3	7	0,13	0,40	3	0,09	0,17	3
319	3	45	239	0	74	84	0,79	0,78	49	1,10	0,59	35
320	0	6	46	0	5	9	0,03	0,19	11	0,06	0,26	10
321	1	17	197	0	34	38	0,61	0,37	24	0,27	0,35	30
322	10	92	371	0	160	169	1,82	1,56	51	0,62	0,67	57
323	0	74	282	0	76	97	0,75	0,42	53	0,45	0,37	42
324	12	94	112	0	92	96	0,42	0,45	70	0,18	0,32	65
325	11	68	594	0	156	201	0,72	1,35	52	0,46	0,45	54
326	3	145	246	0	115	118	0,64	0,91	105	0,33	0,43	97
327	6	230	400	0	106	116	0,97	0,62	55	0,21	0,41	52
328	1	42	63	0	66	77	0,27	0,19	31	0,12	0,28	32
329	7	77	241	0	151	186	0,72	0,78	88	0,44	0,56	70
330	8	106	342	0	191	210	0,82	0,86	54	0,44	0,56	44
331	24	85	427	0	131	147	1,32	0,86	68	0,26	0,40	67
332	18	40	339	0	114	139	0,94	0,89	60	0,13	0,28	54
333	3	84	435	0	136	142	1,19	0,92	83	0,26	0,35	68
334	12	163	267	0	157	169	1,46	1,40	90	0,19	0,51	86

approach reached up to 80% in the best cases (see, for example, the reduction in the standard deviation of 3D-RMSE for the cases DOY 307/2014 and DOY 315/2014). There are few cases (such as DOY 319/2014, presented in Fig. 6) in which the averaged 3D-RMSE produced limited improvement due to successive losses of lock occurring at time intervals shorter than the convergence time (i.e., resonant data gap condition). However, the time series of errors still suggest significant improvement before the occurrence of successive losses of lock affecting more than one link simultaneously. There were few cases with absence of scintillation in the period (such as DOY 314/2014), and for those days, the comparison presented unmeaningful discrepancies of few centimeters that can be fixed at refining steps of our method.

Results also indicate that the impact of strong scintillations in the PPP performance are highly associated with the occurrence of losses of lock and consequently re-initialization of the ambiguity parameter (N_{IF}), but our approach could lead to an overall improvement in the PPP accuracy. Considering averaged values for the 30-days dataset and the application of the three steps of our approach, the standard deviation of 3D-RMSE reduced from 0.79 m to 0.32 m (overall improvement of 59%), and the average of 3D-RMSE reduced from 0.80 m to 0.43 m (overall improvement of 46%). If we consider a partial implementation of the proposed method by applying only steps a and b, the standard deviation of 3D-RMSE reduced to 0.56 m (overall improvement of 29%), and the average of 3D-RMSE reduced to 0.65 m (overall improvement of 19%). The best results were found with the full implementation (application of the three steps). The use of steps a and b separate was not considered because $dScint_{\phi^s_{rIF}}$ and N_{IF} are not independent.

The overall improvement with our method could be augmented by including additional high-rate data, e.g., DLL prompt I_{corr} and Q_{corr} samples in addition to PLL high-rate data. Furthermore, the presence of several losses of lock limited the availability of our proposed corrections for the functional model. In some cases, our method was able to recover the high-accuracy expected to PPP application; however, there are still cases in which the results are still below a desired level required for high-accuracy applications due to resonant data gaps associated to scintillation. Our approach improved the convergence of ambiguities parameter under

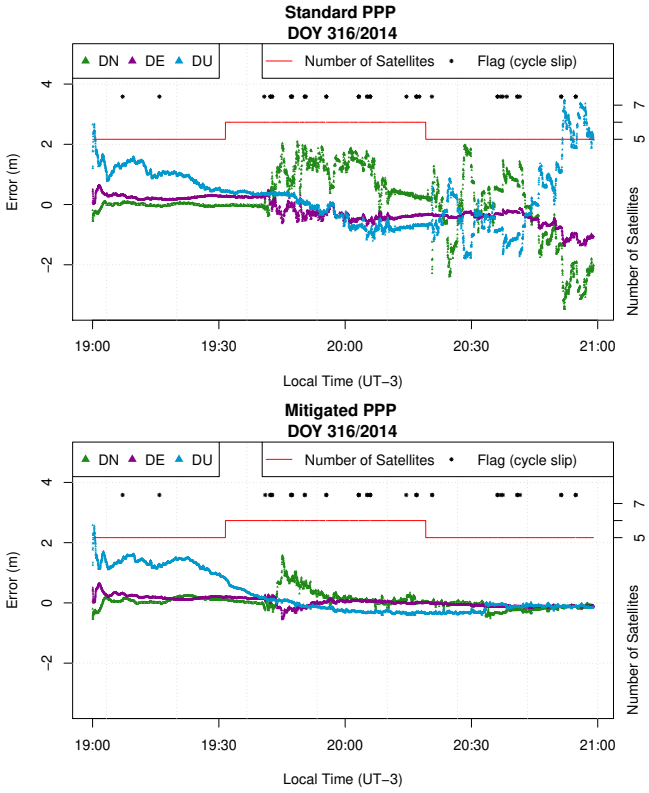

Fig. 5. Comparison between standard (non-mitigated) and mitigated solution for DOY 316/2014. The positional accuracy is presented by the North (DN), East (DE) and Up (DU) error components. The red line indicates the number of satellites and the black dots indicate whether a cycle slip (followed by ambiguity re-initialization) was detected by the PPP software.

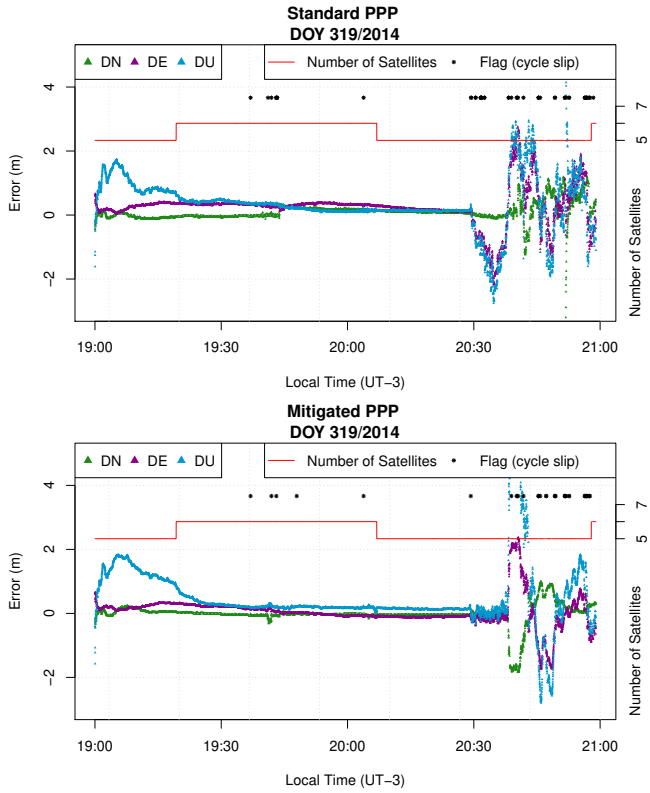

Fig. 6. Comparison between standard (non-mitigated) and mitigated solution for DOY 319/2014. The positional accuracy is presented by the North (DN), East (DE) and Up (DU) error components. The red line indicates the number of satellites and the black dots indicate whether a cycle slip (followed by ambiguity re-initialization) was detected by the PPP software.

influence of strong scintillation, that is reflected in reduction of positioning errors after the ambiguities re-initialization.

In the tests carried out in this work, the RT-PPP software was applied without any modifications in its strategies to deal with cycle slips (e.g., ambiguity re-initialization after a cycle slip is detected by the algorithm presented in [4]. The investigation of improved approaches to manage cycle slips will be a subject of future research, such as the possibility to use the approach presented by [47].

It is to be noted that the novel approach described here can be further improved by utilising additional parameters from the tracking stage of any receiver. In this paper, only high-rate data available from Septentrio PolaRxS receiver with default configuration was applied (50 Hz amplitude and phase for both L1 and L2 at the output of PLL, available only for civil signals). Consequently, the proposed approach could not be fully implemented due to the lack of data, and the corrections and PPP processing were based on limited constellation as they considered only satellites broadcasting L2C signal. We plan to use different receivers (e.g. GISMO) where both PLL/DLL parameters for all the signals can be made available to improve the method in the future. Furthermore, with the proper output from a receiver designed to be loss of lock free, the degradation in the code and phase pseudorange measurements could be better investigated and our method could be refined for different applications demanding high-precise positioning in presence of scintillation, including real time applications

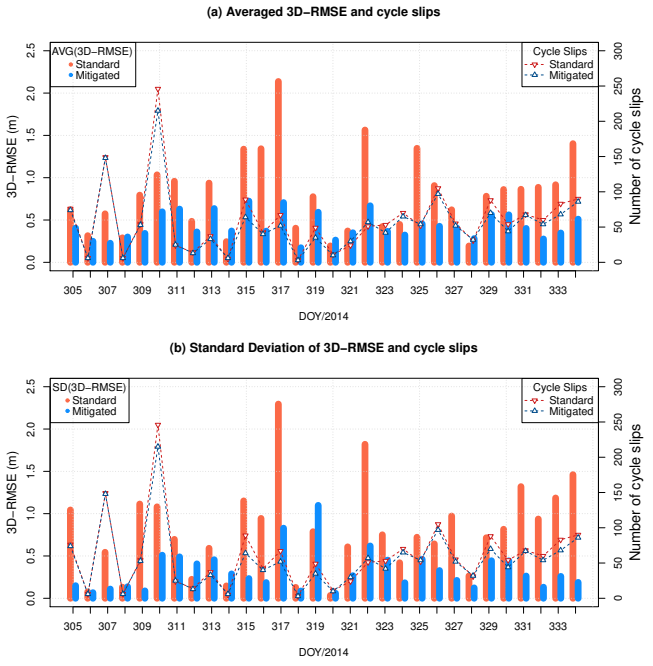

Fig. 7. Plots show day-to-day comparison between the non-mitigated PPP and our mitigation proposed approach. The top plot presents the average of the 3D-RMSE and the bottom plot presents the standard deviation. For not including the initialization period in our analysis, the first 30 minutes of PPP results were not included in RMSE estimation, therefore, each bar represents the period between 19:30 and 21:00 LT. Besides the bars, the dashed triangles demonstrate the number of cycle slips detected by the PPP software (and consequently, the number of ambiguities re-initialization each day).

with kinematic data, such as RTK and differential GNSS. For applications relying on kinematic data, such as autonomous navigation, the proposed method might be adapted or enhanced with additional datasets. Future investigations, such as the analysis of kinematic data and integration with inertial systems can support to depict the scintillation-induced error in presence of fluctuations in the observables originated from the moving antenna. For that case, the proposed approach is still valid, as well as variations relying on the application of the three different steps alternately.

VI. Conclusions

In this paper, we propose a novel approach able to greatly reduce the effects of ionospheric scintillation on PPP, that is the main limitation in achieving high-accuracy GNSS positioning at equatorial latitudes. Our new approach consists of three steps: a) a new functional model that corrects the effects of range errors in the observables; b) a new stochastic model that uses these corrections to generate more accurate positioning; and c) a new strategy to attenuate the effects of losses of lock, thus improving the ambiguities re-convergence caused by the need to re-initialise the tracking.

The effectiveness of our method was demonstrated by using a dataset of 30 days of measurements obtained through GNSS ionospheric monitor in the Brazilian South-Eastern region (static data). These measurements allowed us to combine carrier phases with signals components sampled at 50-Hz sampling rate. In principle, our method can be implemented in any GNSS receiver capable of handling high-rate sampling of carrier phases. Despite the presence of data gaps introduced by scintillation (and corrected through our method), our results demonstrate improvements of up to 80% in the PPP accuracy. We show that, in the best cases, our method can completely negate the effects of ionospheric scintillation and can recover the original PPP accuracy that would have existed without any scintillation.

The significance of this work lies in the improvement it offers in the integrity, reliability and availability of GNSS services and applications that can support several fields of operations, like offshore oil exploration, precision agriculture, mining and autonomous navigation.

Acknowledgment

Monitoring stations from UNESP network were deployed in the context of the Projects CIGALA and CALIBRA (both funded by the European Commission (EC) in the framework of the FP7-GALILEO-2009-GSA and FP7–GALILEO–2011–GSA–1a, respectively), and FAPESP Project Number 06/04008-2. The network is currently supported by National Institute of Science and Technology – GNSS Technology to Support Air Navigation (INCT GNSS-NavAer), funded by CNPq (National Council for Scientific and Technological Development – process 465648/2014-2), FAPESP (Sao Paulo Research Foundation – process 2017/01550-0) and CAPES (Coordination for the Improvement of Higher Education Personnel). Authors thanks to all members of these projects for research collaboration. Bruno Vani thanks for Federal Institute of Education, Science and Technology of Sao Paulo (IFSP) for supporting this PhD research and CAPES for research grant at the University of Bath (CAPES/PDSE n. 19-2016/Process no. 88881.134266/2016-01). A.O. Moraes thanks for the support from CNPq through Award 314043/2018-7. Authors thanks to Eng. David Feng and all the Septentrio's Support Team for collaborative discussions about configurations of PolaRxS receiver.

References

[1] M. Aquino, J. F. G. Monico, A. H. Dodson, H. Marques, G. De Franceschi, L. Alfonsi, V. Romano, and M. Andreotti. Improving the GNSS positioning stochastic model in the presence of ionospheric scintillation. *Journal of Geodesy*, 83(10):953–966, Oct 2009. doi: 10.1007/s00190-009-0313-6.

[2] Santimay Basu, E. MacKenzie, and Sunanda Basu. Ionospheric constraints on VHF/UHF communications links during solar maximum and minimum periods. *Radio Science*, 23(3):363–378, 1988. doi: 10.1029/RS023i003p00363.

[3] H. Berglund. The effects of L2C signal tracking on high-precision carrier phase GPS positioning. *UNAVCO*, 2011. http://kb.unavco.org/kb/article/the-effects-of-l2c-signal-tracking-on-high-precision-carrier-phase-gps-postioning-689.html.

[4] Geoffrey Blewitt. An automatic editing algorithm for GPS data. *Geophysical Research Letters*, 17(3):199–202, 1990. doi: 10.1029/GL017i003p00199.

[5] Johannes Boehm and Harald Schuh. Vienna mapping functions in vlbi analyses. *Geophysical Research Letters*, 31(1):n/a–n/a, 2004. doi: 10.1029/2003GL018984.

[6] BH Briggs and IA Parkin. On the variation of radio star and satellite scintillations with zenith angle. *Journal of Atmospheric and Terrestrial Physics*, 25(6):339–366, 1963. doi: 10.1016/0021-9169(63)90150-8.

[7] Shuyang Cheng, Jinling Wang, and Wenjie Peng. Statistical analysis and quality control for GPS fractional cycle bias and integer recovery clock estimation with raw and combined observation models. *Advances in Space Research*, 60(12):2648–2659, 2017. doi: 10.1016/j.asr.2017.06.053.

[8] Robert S. Conker, M. Bakry El-Arini, Christopher J. Hegarty, and Thomas Hsiao. Modeling the effects of ionospheric scintillation on GPS/satellite-based augmentation system availability. *RADIO SCIENCE*, 38, 2003. doi: 10.1029/2000RS002604.

[9] Zeynep Günsu Elmas. *Exploiting new GNSS signals to monitor, model and mitigate the ionospheric effects in GNSS*. PhD thesis, University of Nottingham, 2013.

[10] Richard D Fontana, Wai Cheung, Paul M Novak, and Thomas A Stansell. The new L2 civil signal. *GPS Joint Program Office*, 2001.

[11] B. Forte. Analysis of the PLL phase error in presence of simulated ionospheric scintillation events. *Radio Science*, 47(3):n/a–n/a, 2012. doi: 10.1029/2011RS004790.

[12] B. Forte and S. M. Radicella. Problems in data treatment for ionospheric scintillation measurements. *Radio Science*, 37(6):8–1–8–5, 2002. doi: 10.1029/2001RS002508.

[13] Luiz Paulo Souto Fortes, Tao Lin, and Gérard Lachapelle. Effects of the 2012–2013 solar maximum on GNSS signals in brazil. *GPS Solutions*, 19(2):309–319, 2015. doi: 10.1007/s10291-014-0389-1.

[14] YANG GAO and XIAOBING SHEN. A new method for carrier-phase-based precise point positioning. *Navigation*, 49(2):109–116, 2002. doi: 10.1002/j.2161-4296.2002.tb00260.x.

[15] Clyde Goad. Surveying with the global positioning system. In *Global Positioning System: Theory and Applications*, pages 501–517. Progress in Astronautics and Aeronautics, 1996. doi: 10.2514/5.9781600866395.0501.0517.

[16] Fei Guo, Xiaohong Zhang, Jinling Wang, and Xiaodong Ren. Modeling and assessment of triple-frequency BDS precise point positioning. *Journal of Geodesy*, 90(11):1223–1235, 2016. doi: 10.1007/s00190-016-0920-y.

[17] Kai Guo, Yang Liu, Yan Zhao, and Jinling Wang. Analysis of ionospheric scintillation characteristics in Sub-Antarctica region with GNSS data at Macquarie Island. *Sensors*, 17(1):137, 2017. doi: 10.3390/s17010137.

[18] Kai Guo, Yan Zhao, Yang Liu, Jinling Wang, Chunxi Zhang, and Yanbo Zhu. Study of ionospheric scintillation characteristics in Australia with GNSS during 2011–2015. *Advances in Space Research*, 59(12):2909–2922, 2017. doi: 10.1016/j.asr.2017.03.007.

[19] Bernhard Hofmann-Wellenhof, Herbert Lichtenegger, and Elmar Wasle. *GNSS – Global Navigation Satellite Systems: GPS, GLONASS, Galileo, and more*. Springer, Berlin; New York, 2008.

[20] Todd E Humphreys, Mark L Psiaki, and Paul M Kintner. Modeling the effects of ionospheric scintillation on GPS carrier phase tracking. *IEEE Transactions on Aerospace and Electronic Systems*, 46(4):1624–1637, 2010. doi: 10.1109/TAES.2010.5595583.

[21] Nathan L Knight, Jinling Wang, and Chris Rizos. Generalised measures of reliability for multiple outliers. *Journal of Geodesy*, 84(10):625–635, 2010. doi: 10.1007/s00190-010-0392-4.

[22] Tao Li, Jinling Wang, and Denis Laurichesse. Modeling and quality control for reliable precise point positioning integer ambiguity resolution with GNSS modernization. *GPS solutions*, 18(3):429–442, 2014. doi: 10.1007/s10291-013-0342-8.

[23] Yang Liu, Lianjie Fu, Jinling Wang, and Chunxi Zhang. Study of GNSS loss of lock characteristics under ionosphere scintillation with GNSS data at Weipa (Australia) during solar maximum phase. *Sensors*, 17(10):2205, 2017. doi: 10.3390/s17102205.

[24] Yang Liu, Lianjie Fu, Jinling Wang, and Chunxi Zhang. Studying ionosphere responses to a geomagnetic storm in june 2015 with multi-constellation observations. *Remote Sensing*, 10(5), 2018. doi: 10.3390/rs10050666.

[25] Haroldo Antonio Marques, João Francisco Galera Monico, Milton Hirokazu Shimabukuro, Rogério Takeshi Oyama, and Jens Peter Wentz. Real time PPP: Fundamentals, computational implementation and results analysis for static and kinematic mode. *Brazilian Cartography Magazine (Revista Brasileira de Cartografia)*, 6(66/6), 2014.

[26] HAS Marques, JFG Monico, and HA Marques. Performance of the l2c civil gps signal under various ionospheric scintillation effects. *GPS solutions*, 20(2):139–149, 2016. doi: 10.1007/s10291-015-0472-2.

[27] Joao Francisco Galera Monico. *Posicionamento pelo GNSS*. Ed. da UNESP, São Paulo, 2008.

[28] Alison de O Moraes, Bruno C Vani, Emanoel Costa, Mangalathayil A Abdu, Eurico R de Paula, Jonas Sousasantos, João FG Monico, Biagio Forte, Patrícia Mara de Siqueira Negreti, and Milton Hirokazu Shimabukuro. GPS availability and positioning issues when the signal paths are aligned with ionospheric plasma bubbles. *GPS Solutions*, 22(4):95, 2018. doi: 10.1007/s10291-018-0760-8.

[29] Marcio T A H Muella, Eurico R de Paula, and Alan A Monteiro. Ionospheric scintillation and dynamics of Fresnel-scale irregularities in the inner region of the equatorial ionization anomaly. *Surveys in Geophysics*, 34(2):233–251, 2013. doi: 10.1007/s10712-012-9212-0.

[30] Alison O. Moraes, Bruno C. Vani, Emanoel Costa, Jonas Sousasantos, Mangalathayil A. Abdu, Fabiano Rodrigues, Yuri C. Gladek, César B. A. Oliveira, and João F. Galera Monico. Ionospheric scintillation fading coefficients for the GPS L1, L2, and L5 frequencies. *Radio Science*, 0(0). doi: 10.1029/2018RS006653.

[31] Alison Oliveira Moraes, Emanoel Costa, Mangalathayil Ali Abdu, Fabiano S. Rodrigues, Eurico Rodrigues de Paula, Kelias Oliveira, and Waldecir João Perrella. The variability of low-latitude ionospheric amplitude and phase scintillation detected by a triple-frequency GPS receiver. *Radio Science*, 52(4):439–460, 2017. doi: 10.1002/2016RS006165.

[32] Alison Oliveira Moraes, Emanoel Costa, Eurico Rodrigues de Paula, Waldecir Joao Perrella, and João Francisco Galera Monico. Extended ionospheric amplitude scintillation model for GPS receivers. *Radio Science*, 49(5):315–329, 2014. doi: 10.1002/2013RS005307.

[33] Alison Oliveira Moraes, Eurico Rodrigues de Paula, Waldecir João Perrella, and Fabiano Silveira Rodrigues. On the distribution of GPS signal amplitudes during low-latitude ionospheric scintillation. *GPS solutions*, 17(4):499–510, 2013. doi: 10.1007/s10291-012-0295-3.

[34] Jihye Park, Sreeja Vadakke Veettil, Marcio Aquino, Lei Yang, and Claudio Cesaroni. Mitigation of ionospheric effects on GNSS positioning at low latitudes. *Navigation*, 64(1):67–74, 2017. doi: 10.1002/navi.177.

[35] L F C Rezende, E R de Paula, I J Kantor, and P M Kintner. Mapping and survey of plasma bubbles over Brazilian territory. *Journal of Navigation*, 60(01):69–81, 2007. doi: 10.1017/S0373463307004006.

[36] Rodrigo Santos Mendes Rocha, Gabriel Oliveira Jerez, Gabriela Oliveira Nascimento Brassarote, and João Francisco Galera Monico. Avaliação do efeito da cintilação ionosférica e de diferentes intervalos de tempo de coleta de dados no posicionamento por ponto preciso na sua forma on-line. *Revista Brasileira de Geomática*, 5(2):251–276, 2017. doi: 10.3895/rbgeo.v5n2.5429.

[37] Septentrio Satellite Navigation, Leuven, Belgium. *PolaRxS Application Manual*, March 2015.

[38] Heloisa Alves Silva, Paulo Oliveira Camargo, João Francisco Galera Monico, Marcio Aquino, Haroldo Antonio Marques, Giorgiana De Franceschi, and Alan Dodson. Stochastic modelling considering ionospheric scintillation effects on GNSS relative and point positioning. *Advances in Space Research*, 45(9):1113 – 1121, 2010. Special Issue: Recent Advances in Space Weather Monitoring, Modelling, and Forecasting. doi: 10.1016/j.asr.2009.10.009.

[39] L. Siniscalco, N. Pastori, A. Zin, A. Emmanuele, A. Ferrario, C. Manno, and B. Forte. GISMO: A smart sensor to mitigate and monitor ionospheric effects. In *Proceedings of the 30th International Technical Meeting of The Satellite Division of the Institute of Navigation (ION GNSS+ 2017)*, pages 2263 – 2272, Portland, Oregon, September 2017. https://www.ion.org/publications/abstract.cfm?articleID=15331.

[40] Luca Spogli, Lucilla Alfonsi, Vincenzo Romano, Giorgiana De Franceschi, Galera Monico Joao Francisco, Milton Hirokazu Shimabukuro, Bruno Bougard, and Marcio Aquino. Assessing the GNSS scintillation climate over Brazil under increasing solar activity. *Journal of Atmospheric and Solar-Terrestrial Physics*, 105:199–206, 2013. doi: 10.1016/j.jastp.2013.10.003.

[41] V. Sreeja, M. Aquino, Z. G. Elmas, and B. Forte. Correlation analysis between ionospheric scintillation levels and receiver tracking performance. *Space Weather*, 10(6):n/a–n/a, 2012. doi: 10.1029/2012SW000769.

[42] A. J. Van Dierendonck, J. A. Klobuchar, and Q. Hua. Ionospheric scintillation monitoring using commercial single frequency C/A code receivers. In *Proceedings of the Institute of Navigation*, volume 93, pages 1324–1333, Alexandria (VA), 1993.

[43] Bruno César Vani, Milton Hirokazu Shimabukuro, and João Francisco Galera Monico. Visual exploration and analysis of ionospheric scintillation monitoring data: The ISMR query tool. *Computers & Geosciences*, 104:125–134, 2017. doi: 10.1016/j.cageo.2016.08.022.

[44] Michel Daoud Yacoub. *Foundations of mobile radio engineering*. CRC press, 1993.

[45] Michel Daoud Yacoub. The alpha-mu distribution: A physical fading model for the Stacy distribution. *IEEE Transactions on Vehicular Technology*, 56(1):27–34, 2007. doi: 10.1109/TVT.2006.883753.

[46] Ling Yang, Jinling Wang, Nathan L Knight, and Yunzhong Shen. Outlier separability analysis with a multiple alternative hypotheses test. *Journal of Geodesy*, 87(6):591–604, 2013. doi: 10.1007/s00190-013-0629-0.

[47] Xiaohong Zhang, Fei Guo, and Peiyuan Zhou. Improved precise point positioning in the presence of ionospheric scintillation. *GPS solutions*, 18(1):51–60, 2014. doi: 10.1007/s10291-012-0309-1.

[48] J. F. Zumberge, M. B. Heflin, D. C. Jefferson, M. M. Watkins, and F. H. Webb. Precise point positioning for the efficient and robust analysis of GPS data from large networks. *Journal of Geophysical Research: Solid Earth*, 102(B3):5005–5017, 1997. doi: 10.1029/96JB03860.